Published in final edited form as:
Cell. 2014 April 10; 157(2): 433–446. doi:10.1016/j.cell.2014.01.067.

Intestinal brush border assembly driven by protocadherin-based intermicrovillar adhesion

Scott W. Crawley[1], **David A. Shifrin Jr.**[1], **Nathan E. Grega-Larson**[1], **Russell E. McConnell**[1], **Andrew E. Benesh**[1], **Suli Mao**[1], **Yuxi Zheng**[2], **Qing Yin Zheng**[2], **Ki Taek Nam**[3], **Bryan A. Millis**[4], **Bechara Kachar**[4], and **Matthew J. Tyska**[1]

[1]Department of Cell and Developmental Biology, Vanderbilt University Medical Center, Nashville, TN 37232, USA

[2]Department of Otolaryngology-HNS, Case Western Reserve University, Cleveland, OH 44106, USA

[3]Severance Biomedical Science Institute, Yonsei University College of Medicine, Seoul 120-752, Korea

[4]National Institute on Deafness and Other Communication Disorders, National Institutes of Health, Bethesda, MD 20892, USA

Abstract

Transporting epithelial cells build apical microvilli to increase membrane surface area and enhance absorptive capacity. The intestinal brush border provides an elaborate example, with tightly packed microvilli that function in nutrient absorption and host defense. Although the brush border is essential for physiological homeostasis, its assembly is poorly understood. We found that brush border assembly is driven by the formation of Ca^{2+}-dependent adhesion links between adjacent microvilli. Intermicrovillar links are composed of protocadherin-24 and mucin-like protocadherin, which target to microvillar tips and interact to form a *trans* heterophilic complex. The cytoplasmic domains of microvillar protocadherins interact with the scaffolding protein, harmonin, and myosin-7b, which promote localization to microvillar tips. Finally, a mouse model of Usher syndrome lacking harmonin exhibits microvillar protocadherin mislocalization and severe defects in brush border morphology. These data reveal an adhesion-based mechanism for brush border assembly and illuminate the basis of intestinal pathology in Usher syndrome patients.

Keywords

actin; myosin; intestine; epithelia; polarity; membrane; protrusion

Correspondence should be addressed to: Matthew J. Tyska, Ph.D. Associate Professor of Cell and Developmental Biology Vanderbilt University Medical Center 3154 Medical Research Building III 465 21st Ave. South Nashville, TN 37232 matthew.tyska@vanderbilt.edu.

INTRODUCTION

Enterocytes are transporting epithelial cells that line the luminal surface of the intestinal tract where they function in nutrient processing, absorption, and host defense. One of the defining features of terminally differentiated enterocytes is the densely packed array of microvilli known as the brush border (BB), which extends from the apical surface into the lumen. BB microvilli are actin bundle-supported membrane protrusions that exhibit striking uniformity in length and are maximally packed in a hexagonal pattern such that a single cell presents up to ~1000 of these protrusions (Mooseker, 1985). This unique morphology allows enterocytes to maintain a vast reservoir of membrane enriched in nutrient processing and transport machinery on their apical surface (Maroux et al., 1988). In addition to functioning as the sole site of nutrient absorption, the BB also plays an active role in defending host tissues against luminal microbes and microbial toxins (Mukherjee et al., 2008; Selsted and Ouellette, 2005; Shifrin and Tyska, 2012).

Due to the constant regenerative renewal of the gut epithelium, enterocyte differentiation and BB assembly are processes that continue throughout our lifetime. Differentiation occurs as enterocytes migrate along the crypt-villus axis, during which time they exhibit a marked up-regulation of cytoskeletal genes including actin, villin and espin (Chang et al., 2008; Mariadason et al., 2005), changes which likely contribute to BB assembly. Despite the development and characterization of numerous animal models lacking key BB components (Revenu et al., 2012; Saotome et al., 2004; Tyska et al., 2005), little is known about how the BB is assembled during enterocyte differentiation. Fundamental questions on how microvillar actin filaments are nucleated, how microvillar length is regulated, and how these protrusions achieve dense packing during BB assembly remain unanswered.

Adhesion molecules play essential roles in numerous biological processes including the organization of cells during tissue morphogenesis (Guillot and Lecuit, 2013), and in the development and function of stereocilia, specialized mechanosensory protrusions on the surface of inner ear sensory cells (Kazmierczak et al., 2007). Usher syndrome is a major form of inherited deaf-blindness that is caused by loss-of-function mutations in components of the stereocilia Ca^{2+}-dependent adhesion complex, which includes protocadherins and the scaffolding protein, harmonin (Pan and Zhang, 2012). Although primarily viewed as a sensory disorder, Type 1 Usher syndrome patients with mutations in harmonin present with enteropathy and perturbations in villus morphology (Bitner-Glindzicz et al., 2000). However, the cellular basis for this pathology and, more generally, the role of adhesion molecules in the assembly and organization of the BB have not been investigated.

Here, we report that cadherin family adhesion proteins play a critical role in the assembly and organization of the BB. We show that microvilli on the surface of native and cultured intestinal epithelial cells are organized by an extensive matrix of ~50 nm protocadherin-based links, which connect adjacent protrusions in a Ca^{2+}-dependent manner. Furthermore, we find that harmonin functions in the targeting of these protocadherins and is also essential for BB assembly. Our data suggest a model for BB assembly whereby protocadherin-dependent adhesion drives the clustering of microvilli, which leads to the tight packing and uniform length of protrusions in terminally differentiated enterocytes. These findings

suggest a critical role for adhesion molecules in shaping the intestinal epithelial surface and may help develop our understanding of intestinal pathologies associated with inherited, infectious, or iatrogenic causes.

RESULTS

Microvilli cluster and are connected by Ca^{2+}-dependent thread-like links during BB assembly

To gain insight on the mechanism of BB assembly, we imaged the apical surface ultrastructure of CACO-2_{BBE} cells differentiating in culture and native gut epithelium isolated from adult mice. To our knowledge, CACO-2_{BBE} is the only cell line that takes on both morphological and biochemical attributes of *bona fide* enterocytes following prolonged period of differentiation in culture (Peterson and Mooseker, 1992). CACO-2_{BBE} cells were grown on Transwell filters and processed for SEM over a range of post-confluency time points (Fig. 1A). At two days post-confluency (DPC), cells exhibited sparse microvilli that were highly variable in length, with some protrusions appearing only as small buds on the apical membrane (Fig. 1A, DPC2 arrows). Strikingly, microvilli clustered together at this time point and exhibited apparent adhesion between distal tips (Fig. 1A, DPC2 arrowheads). At four DPC (Fig. 1A, DPC4), cells displayed numerous clusters that were disorganized, but contained more protrusions than early time points (10-20 microvilli per cluster). At eight DPC (Fig. 1A, DPC8), many cells showed large, well organized clusters (50-80 microvilli) separated by regions of apical membrane that were free of protrusions. Positioning of microvillar clusters on the apical surface was variable with no obvious organizing center (Fig. S1A left panel). CACO-2_{BBE} cells observed at 20-DPC exhibited fully differentiated BBs with microvilli that were uniform in length and maximally packed, as indicated by the pronounced hexagonal pattern across the monolayer (Fig. 1A, DPC20; Fig. S1A right panel).

Higher magnification imaging unexpectedly revealed that clustering microvilli were physically connected by small, thread-like links (Fig. 1B). Such intermicrovillar links have not been described before, but were observed at both early and late time points. On the surface of 4-DPC CACO-2_{BBE} cells, we observed thread-like links connecting the distal tips of adjacent microvilli; more proximal links were also observed (Fig. 1B, DPC4 arrows). Potentially partial or broken links were also evident along the microvillar axis (Fig. 1B, DPC4 arrowheads). At the later 20-DPC time point, an extensive and highly ordered network of thread-like links connected adjacent microvilli (Fig. 1B, DPC20). Brief treatment of monolayers with the Ca^{2+} chelator BAPTA, or proteinase K nearly eliminated intermicrovillar links, while treatment with a mixture of glycosidases had no effect (Fig. S1B). Thus, intermicrovillar links are likely Ca^{2+}-dependent protein complexes.

To determine if native enterocytes possessed structural features similar to the intermicrovillar links observed in CACO-2_{BBE} cultures, we prepared both mouse intestinal tissue and 20-DPC CACO-2_{BBE} cells for analysis using freeze-etch electron microscopy. Tissue samples prepared from mouse duodenum revealed an extensive network of intermicrovillar links that were similar in appearance and organization to those observed in 20-DPC CACO-2_{BBE} cultures (Fig. 1B; Fig. S1C). Mean link length measured in native

tissue freeze-etch images (46.8 ± 8.9 nm, n = 297) was comparable to those observed for CACO-2_{BBE} cells imaged using the same method (49.9 ± 8.8 nm, n = 361)(Fig. 1C). Together, these results led us to hypothesize that intermicrovillar links provide a physical basis for microvillar clustering during BB assembly.

Enterocytes express two candidate intermicrovillar adhesion molecules

Our finding that microvilli are physically connected by Ca^{2+}-dependent protein complexes immediately suggested cadherins as possible molecular constituents of intermicrovillar links (Brasch et al., 2012). The BB proteome contains four members of the cadherin superfamily: mucin-like protocadherin (MLPCDH), protocadherin-24 (PCDH24), E-cadherin, and cadherin-17 (McConnell et al., 2011). Because E-cadherin and cadherin-17 localize specifically to the basolateral compartment (Fig. S2A)(Berndorff et al., 1994; Boller et al., 1985), further studies focused on MLPCDH and PCDH24. Analysis of MLPCDH and PCDH24 localization in human duodenal tissue revealed high expression in enterocytes along the villus axis, with much lower levels in crypts (Fig. 2A). Heat maps of fluorescence signal revealed marked enrichment of MLPCDH and PCDH24 towards the distal tips of BB microvilli (Fig. 2A zoom panels). The apical targeting of both proteins was confirmed in CACO-2_{BBE} monolayers, where MLPCDH and PCDH24 were found exclusively in the BB (Fig. 2B).

Analysis of microvillar clustering relative to MLPCDH or PCDH24 expression levels in CACO-2_{BBE} cells revealed that MLPCDH is expressed uniformly across monolayers, in both clustering and non-clustering microvilli (Fig. 2C top). In contrast, PCDH24 expression is more mosaic with levels that are highly correlated with the appearance of robust microvillar clustering (Fig. 2C bottom). PCDH24 also exhibits striking enrichment at the tips of clustering microvilli and at points of contact between adjacent protrusions (Fig. 2D). PCDH24 occupied the distal ~20% of CACO-2_{BBE} microvilli (Fig. S2B). To gain more detailed insight on the localization of PCDH24 relative to intermicrovillar links, we prepared 12-DPC CACO-2_{BBE} monolayers for immuno-TEM using an antibody directed against the PCDH24 extracellular domain (Fig. 2E,F). Gold particles were typically found near the distal tips of microvilli and links that connected adjacent microvilli were frequently labeled with one or two particles (Fig. 2E; Fig. S2C). These data suggest that PCDH24 is properly positioned to contribute to the formation of intermicrovillar links.

PCDH24 is required for microvillar clustering and length uniformity

To determine if PCDH24 plays a role in the formation of intermicrovillar links or the clustering of microvilli during BB assembly, we created knockdown (KD) CACO-2_{BBE} cell lines using lentivirus-mediated stable transduction (Fig. S3A,B). Scoring cells from 12-DPC monolayers for microvillar clustering showed that KD of PCDH24 resulted in a dramatic loss of clustering (Fig. 3A,B). Cells expressing a negative control exhibited normal clustering, similar to non-transduced monolayers. Importantly, expression of a PCDH24-EGFP construct refractory to KD rescued clustering, confirming specificity of the phenotype (Fig. 3A,B). In contrast, expression of a rescue construct lacking the first extracellular cadherin (EC) repeat (ΔEC1-PCDH24-EGFP), which is predicted to ablate adhesion function (Nose et al., 1990), failed to rescue clustering (Fig. 3A,B).

SEM of 8-DPC scramble control CACO-2_{BBE} cells revealed organized clusters of microvilli separated by free apical space, similar to non-transduced cells (Fig. S3D, top panels). PCDH24 KD cells failed to exhibit organized clustering and possessed microvilli that displayed seemingly random contact (Fig. S3D, bottom panels). In control cells, organized microvillar clustering was followed by the development of well-formed BBs by 20-DPC (Fig 3C, top panels); these structures also exhibited the characteristic hexagonal packing and uniform length of microvilli. As with non-transduced cells, discrete physical links between adjacent microvilli were observed (Fig. 3C, zoom inset). PCDH24 knockdown gave rise to BBs that were strikingly disheveled in appearance at the 20-DPC time point, with fewer loosely packed microvilli that were highly variable in length and lacked observable intermicrovillar links (Fig. 3C bottom panels; Fig. 3D,E). These studies indicate that PCDH24 is necessary for the formation of intermicrovillar links, as well as tight microvillar packing and length regulation during CACO-2_{BBE} differentiation.

We also examined the impact of PCDH24 overexpression on microvillar clustering in CACO-2_{BBE} monolayers. Overexpression of PCDH24-EGFP induced microvillar clustering in 12-DPC monolayers, while overexpression of a control F-actin marker, UtrCH-EGFP (Burkel et al., 2007), had no effect on clustering (Fig. S3E,F). Expression of ΔEC1-PCDH24-EGFP had a dominant negative effect and abolished observable microvillar clustering (Fig. S3E,F). These results suggest that PCDH24 expression can drive microvillar clustering during BB assembly.

PCDH24 and MLPCDH interact to form Ca^{2+}-dependent heterophilic adhesion complexes *in vitro*

To promote the clustering of adjacent microvilli, PCDH24 could function as a *bona fide* adhesion molecule, although little is known about the adhesive properties of this cadherin family member. To probe the adhesion potential of PCDH24, we performed bead aggregation assays (Emond et al., 2011). Full-length PCDH24 ectodomain (ED) was expressed in HEK293T cells as an Fc domain fusion, isolated and used to coat fluorescent protein-A beads (Fig. 4A; Fig. S4A). As a positive control and point of comparison, E-cadherin ED-coated beads were also examined. PCDH24 ED-coated beads did exhibit time-dependent aggregation, but clusters were significantly smaller than those mediated by E-cadherin ED indicating weak homophilic adhesion (Fig. 4B,C).

Given the weak homophilic adhesion mediated by PCDH24, we explored the possibility that intermicrovillar links represent heterophilic adhesion complexes composed of PCDH24 and some other BB membrane component. This configuration would be similar to that described for hair cell stereocilia, where tip-links are formed by heterophilic interactions between cadherin-23 (CDH23) and protocadherin-15 (PCDH15)(Kazmierczak et al., 2007). We tested for interactions between PCDH24 and the two splice forms of MLCPDH that are found in the BB. The long form of MLPCDH (MLPCDH-L) is identical to the short isoform (MLPCDH-S) with the exception that it contains juxtamembrane mucin-like repeats (Fig. 4A)(Goldberg et al., 2000). Beads coated with either MLPCDH-L or MLPCDH-S ED alone did not aggregate, indicating that MLPCDH isoforms are incapable of homophilic adhesion (Fig. S4B). However, mixtures of PCDH24-coated and MLPCDH-coated beads produced

large aggregates, demonstrating that PCDH24-MLPCDH heterophilic interactions are significantly stronger than PCDH24 homophilic binding (Fig 4B,C). Deletion of the first EC domain of PCDH24 abolished both homophilic binding and heterophilic interactions with both isoforms of MLPCDH, implicating the PCDH24 N-terminus in adhesion bond formation. Importantly, removal of Ca^{2+} using EGTA eliminated all interactions between PCDH24-and MLPCDH-coated beads (Fig. 4B).

Using pull-down assays performed under stringent conditions, we further characterized the homophilic and heterophilic interactions mediated by PCDH24. We generated 6×His and FLAG-tagged EDs from PCDH24 and both isoforms of MLPCDH (Fig. 4A).. Co-incubation of differentially tagged versions of PCDH24 did not reveal homophilic interactions by pull-down analysis, most likely because the interaction is too weak to be detected by this method (Fig. 4D). PCDH24 was found, however, to interact strongly with both isoforms of MLPCDH (Fig. 4D). This interaction was again specific to the PCDH24 N-terminus, as deletion of the first EC domain abolished binding. Thus, PCDH24 and MLPCDH interact in *trans* to form Ca^{2+}-dependent adhesion complexes.

PCDH24-MLPCDH *trans*-heterophilic complexes formed *in vitro* are morphologically similar to intermicrovillar links

If PCDH24 and MLPCDH interact in *trans* to form adhesion complexes that link adjacent microvilli, the heterophilic complexes formed *in vitro* (Fig. 4B,D) should exhibit morphology comparable to intermicrovillar links. To test this prediction, protein A-conjugated magnetic beads were coated with EDs from PCDH24, MLPCDH-L, or MLPCDH-S and examined with SEM. PCDH24-coated samples exhibited an extensive network of *intra-bead* thread-like links (Fig. S4C left panels, arrows). These structures were likely the result of PCDH24 *trans*-homophilic interactions, as beads coated with ΔEC1-PCDH24 ED lacked such features (not shown). Consistent with the bead aggregation and pull-down assays described above, no such structures were observed on the surface of beads coated with EDs from MLPCDH-L or MLPCDH-S (Fig. S4C right panels, arrowheads). Importantly, the differential surface appearance of these bead preparations enabled us to unambiguously assign the identities of beads in samples where PCDH24- and MLPCDH-coated beads were mixed together (Fig. S4D). Samples containing both PCDH24- and MLPCDH-coated beads demonstrated extensive *inter-bead* links, which were similar in morphology to intermicrovillar links (Fig. 4E). These *in vitro* reconstitution results lead us to propose that intermicrovillar links observed on the surface of CACO-2_{BBE} cells and native enterocytes are composed, at least in part, by the PCDH24-MLPCDH complexes characterized here. Such heterophilic complexes would contain 12 EC domains (~4.5 nm each)(Boggon et al., 2002) and thus, extend to a predicted length of ~54 nm if they bind end-to-end or slightly less if there is overlap between N-terminal EC domains (Sotomayor et al., 2012). This value is strikingly similar to the mean intermicrovillar link lengths measured from CACO-2_{BBE} cells and native small intestine (Fig. 1B,C).

If PCDH24 and MLPCDH interact to produce adhesion that drives the packing of microvilli during BB assembly, these molecules should colocalize at the tips of clustering microvilli on the surface of differentiating CACO-2_{BBE} cells. Consistent with this prediction, triple

labeling of samples showed robust colocalization of MLPCDH and PCDH24 at the tips of clustered microvilli (Fig. 5A, white puncta). Immuno-gold labeling for MLPCDH confirmed distal tip targeting in CACO-2_{BBE} microvilli, with gold particles often labeling intermicrovillar links (Fig. 5B,C). We also investigated whether MLPCDH KD impacted microvillar clustering in CACO-2_{BBE} cells (Fig. S3A,C). Similar to PCDH24 KD, loss of MLPCDH resulted in a dramatic reduction of microvillar clustering (Fig. 5D,F). Expression of a refractory construct of either isoform of MLPCDH rescued the clustering defect, with the short isoform exhibiting a complete rescue. Mutation of a critical arginine residue of MLPCDH (R109G), which is predicted to be necessary for adhesive function (Sotomayor et al., 2012), eliminated binding to PCDH24 *in vitro* and rescue of microvillar clustering in cells (Fig. 5D-F). These data lead us to propose a model where PCDH24 and MLPCDH interact at the tips of neighboring microvilli to form intermicrovillar links, which drive the packing of these structures during BB assembly.

Microvillar protocadherins form a complex with harmonin and the actin-based motor, myosin-7b

To develop further insight on the mechanism of adhesion complex formation at microvillar tips, we used biochemical pull-downs and recently published BB proteome data (McConnell et al., 2011) to search for proteins that interact with the cytoplasmic domains (CD) of PCDH24 and MLPCDH. Pull-downs revealed that the PCDH24 and MLPCDH CDs interact with the scaffolding protein, harmonin (Fig. 6A). Also known as ‘AIE-75’ due to its association with Auto-Immune Enteropathy (Kobayashi et al., 1999), and ‘Ush1c’ due to its linkage to Type 1 Usher syndrome (Bitner-Glindzicz et al., 2000; Verpy et al., 2000), harmonin is expressed in at least three splice variants (a, b, and c). Harmonin-a contains three PDZ domains and a coiled-coil region with the potential for dimerization, and based on western blots of CACO-2_{BBE} cell lysates and BBs isolated from mouse duodenal tissue is likely the principle isoform expressed in gut (Fig. S5A,C,D)(Kobayashi et al., 1999). Fine mapping studies indicate that PCDH24 and MLPCDH CDs both bind strongly to the first PDZ domain (Fig. 6B,C). Mutation of the canonical C-terminal PDZ-binding motifs of PCDH24 and MLPCDH (L1310R and I845R, respectively) almost completely ablated these interactions. Consistent with early work (Kobayashi et al., 1999), we found that harmonin-a is highly expressed along the full length of the intestinal tract, with intense staining in the BB (Fig. S5B). Moreover, this molecule is specifically enriched at the distal tips of microvilli (Fig. 6E,G). Thus, harmonin-a is well positioned to interact with PCDH24 and MLPCDH CDs in the BB.

Transmembrane proteins interact with the underlying cytoskeleton to stabilize their sub-cellular localization (Nelson and Veshnock, 1987; Tyska and Mooseker, 2004). In the cochlea, harmonin-b, interacts with CDH23 and functions in maintaining upper tip-link position, in part by binding to F-actin (Boeda et al., 2002; Grati and Kachar, 2011; Grillet et al., 2009; Siemens et al., 2002). Within the microvillus, some other factor would be required to mediate interactions with the core bundle as harmonin-a does not bind to actin (Boeda et al., 2002). PDZ domain-containing proteins can interact with myosin motors, which could provide a link to the actin cytoskeleton (Belyantseva et al., 2005; Boeda et al., 2002). Although the BB is home to several myosin isoforms (McConnell et al., 2011), we chose to

focus on myosin-7b (Myo7b) because this motor is enriched in the distal half of microvilli (Chen et al., 2001). Myo7b possesses a cargo-binding domain that consists of tandem MyTH4-FERM domains separated by a single SH3 domain (Chen et al., 2001). Pull-downs showed that the cargo-binding domain of Myo7b does interact with harmonin-a, with PDZ2 being the preferred binding site (Fig. 6D). We also found that the tail domain of Myo7b binds to the CDs of both PCDH24 and MLPCDH (Fig. 6A). Finally, localization studies revealed that Myo7b is expressed along the intestinal tract where it exhibits enrichment in the BB and targets specifically to distal tips of microvilli (Fig. S5B; Fig. 6F,H). Thus, Myo7b is positioned to link harmonin, PCDH24, and MLPCDH to the distal tip of the actin core bundle (Fig. 6I).

Protocadherin binding to harmonin is required for normal microvillar clustering in CACO-2_{BBE} cells

Our results suggest that harmonin serves as a hub of molecular interactions between the transmembrane microvillar protocadherins and Myo7b, which can bind directly to the actin core. If this is the case, disrupting interactions with harmonin should perturb the function of PCDH24 and MLPCDH by preventing their proper targeting to microvillar tips. To test this prediction, we first determined the impact of CD deletion. A PCDH24 construct lacking the CD (PCDH24-ΔCD-EGFP) was unable to interact with Myo7b, target properly, or promote microvillar clustering in CACO-2_{BBE} cells (Fig. S6A-D). To determine if a loss of harmonin binding was sufficient to explain the lack of targeting, we created a variant of PCDH24 where the CD was replaced with an in-frame fusion to harmonin-a (PCDH24-ΔCD-Harm-EGFP). Remarkably, this chimera regained binding to Myo7b, showed strong distal tip enrichment, and promoted microvillar clustering (Fig. S6A-D). Thus, harmonin binding to the CD of PCDH24 promotes the targeting of this molecule to the distal tip, potentially by mediating interactions with Myo7b.

A MLPCDH construct lacking the CD (MLPCDH-S-ΔCD-EGFP) failed to target efficiently or promote microvillar clustering in MLPCDH KD cells (Fig. S6E-G). A chimera of MLPCDH where the CD was replaced with full-length harmonin (MLPCDH-S-ΔCD-Harm-EGFP) was also unable to rescue the KD phenotype. However, fusion of a truncated version of harmonin encoding the second and third PDZ domains (MLPCDH-S-ΔCD-PDZ23-EGFP) resulted in a partial rescue (Fig. S6E-G). The MLPCDH-S-ΔCD-PDZ23-EGFP chimera exhibited robust BB localization, but only promoted the formation of small clusters (Fig. S6F,H). In combination with experiments on PCDH24 chimeras (Fig. S6A-D), these data indicate that the interaction between microvillar protocadherins and harmonin is necessary for proper BB assembly in CACO-2_{BBE} cells.

Loss of harmonin disrupts BB assembly *in vivo*

We also examined the functional significance of harmonin and its interactions with microvillar protocadherins *in vivo* by investigating the harmonin KO mouse, a model for Type 1 Usher syndrome (Tian et al., 2010). Mice lacking harmonin exhibit a striking redistribution of Myo7b out of the BB, with signal that is enriched in the cytoplasm (Fig. 7A,B; Fig. S7A). Thus, Myo7b targeting to microvillar tips is dependent on harmonin. Harmonin KO animals also lack the distal tip enrichment of MLPCDH typically observed in

WT tissue, and instead exhibit signal that is more broadly distributed along the microvillar axis (Fig. 7C,D). Thus, while MLPCDH trafficking to the BB does not depend on harmonin or Myo7b, MLPCDH enrichment at microvillar tips depends on harmonin.

To investigate how loss of harmonin impacts BB morphology, we performed SEM on KO tissues. We found gross perturbations to epithelial cell morphology in both the small intestine and proximal colon of KO animals (Fig. 7E,F). KO enterocytes and colonocytes exhibited defects in apical morphology that were strikingly similar to PCDH24 KD CACO-2_{BBE} cells; microvilli were short and irregular in shape, and lacked the tight packing that is characteristic of native BBs (Fig. 7E,F zoom panels; Fig. 7G,H). BB defects, however, appeared in a mosaic fashion, most likely the result of heterogeneity in the numerous crypts that generate epithelial cells for a given villus (e.g. different crypts might generate cells that express different levels of phenotype-limiting factors). Scoring revealed ~10% of enterocytes and ~40% of colonocytes exhibited a significant disruption in BB morphology, whereas ~35% of colonocytes appeared to lack BBs entirely (Fig. 7H). Intermicrovillar links are still present in BBs with severe morphological defects, although they are disorganized and no longer localized specifically to the tips of microvilli (Fig. S7B). This suggests that tip localization of adhesion complexes plays a central role in microvillar organization. Moreover, in the small intestine, BB defects are observed along the full length of the villus and even impact cells that are newly emerged from the crypt (e.g. at the base of the villus; data not shown). Thus, observed phenotypes most likely represent defects in initial BB assembly rather than maintenance. In combination, these studies reveal that in the absence of harmonin, Myo7b and MLPCDH are no longer enriched at microvillar tips and this is associated with perturbations in BB morphology along the length of the intestinal tract.

The extensive defects in BB structure observed in KO colon are coupled to a significant reduction in proliferation (Fig. S7C,D). Given the intricate feedback mechanisms that link proliferation and differentiation in the intestinal epithelium, this finding might reflect a problem with the maturation of colonocytes as they emerge from the crypt. Beyond this perturbation, loss of harmonin function in KO mice appears to be compensated to the extent that animal physiology is not impaired (Fig. S7E-I). This result is expected given the overbuilt nature of the gut (Jeejeebhoy, 2002) and the incomplete penetrance of BB perturbations; it is also reminiscent of studies with other mouse models lacking major BB structural components (e.g. myosin-1a, villin, espin, or fimbrin), all of which exhibit mild or undetectable physiological effects (Ferrary et al., 1999; Grimm-Gunter et al., 2009; Revenu et al., 2012; Tyska et al., 2005).

DISCUSSION

A new model for BB assembly

Based on the findings presented here, we propose a model where Ca^{2+}-dependent extracellular adhesion drives the assembly of the BB during epithelial differentiation (Fig. S7J). PCDH24 and MLPCDH are expressed during enterocyte (or colonocyte) differentiation and delivered to the apical face of the cell via the secretory pathway. Once integrated into the apical membrane, the CDs of both PCDH24 and MLPCDH interact with

harmonin-a and Myo7b, forming a complex that is needed for enrichment at microvillar tips. Microvillar protocadherins then interact in *trans* to form adhesion complexes that drive the coalescence of adjacent microvilli into clusters. Such clusters are small early in differentiation, but grow dramatically by incorporating more protrusions as differentiation proceeds. As a cell approaches a terminally differentiated state, the apical surface contains one or very few large-scale microvillar clusters, i.e. a fully assembled BB. Thus, intermicrovillar adhesion provides a mechanism to solve the tight packing problem from a time point early in differentiation. Clustering microvilli in this way would also create large areas of 'free' apical membrane where nascent microvilli might more readily emerge (Fig. 1A, 2-8 DPC time points).

Tip localization of adhesion complexes is a critical feature of this model; if adhesion complexes were allowed to form and localize along the length of microvilli, clustering would become disorganized, e.g. the tip of one microvillus could interact with the base of another. This model also requires that microvilli on the surface of differentiating epithelial cells are dynamic, such that smaller pre-existing clusters might collide and coalesce into a single large cluster during BB assembly. Although such dynamics have not been described before, imaging apical surface remodeling during epithelial differentiation is a clear goal of future studies.

Functional implications of intermicrovillar adhesion

In addition to organizing the tight packing of BB microvilli, intermicrovillar links also function in controlling microvillar dimensions, as KD of PCDH24 and KO of harmonin increased variability in microvillar length (Fig. 3C and Fig 7E,F bottom panels). These findings are reminiscent of previous studies showing that over-expression of *Drosophila* Cad99C influences microvillar length on the surface of ovarian follicle cells (D'Alterio et al., 2005; Schlichting et al., 2006). Formation of adhesion complexes between the tips of adjacent microvilli might enable the physical communication of length information across the BB, promoting uniformity in length. How the absolute length of microvilli is controlled during differentiation remains unclear. Additional studies are needed to determine if the length control mechanisms that operate in other protrusions, such as the cilium, are active in the BB (Chan and Marshall, 2012).

The extensive network of intermicrovillar links may also play a role in stabilizing the BB against mechanical forces. The BB must be robust enough to withstand continuous mechanical insults imposed by the phasic smooth muscle contraction of peristalsis. Intermicrovillar adhesion could serve to resist such forces and to promote long-term stability of BB morphology. Moreover, the Ca^{2+}-dependence of intermicrovillar adhesion suggests that factors that modulate free Ca^{2+} in the lumen, i.e. diet or exposure to chelating agents (e.g. radiocontrast agents)(Widmark, 2007), are expected to have a severe impact on BB assembly and stability.

Parallels with the inner ear sensory epithelium

A striking parallel to intermicrovillar adhesion is found at the tips of stereocilia, the actin-based protrusions that extend from the surface of cochlear and vestibular hair cells to detect

mechanical forces evoked by sound energy and head movement. In this specialized context, stereocilia from a single hair cell are organized into a “hair bundle” consisting of rows of precisely defined heights forming a characteristic staircase pattern (Schwander et al., 2010). Stereocilia are connected to their neighbors by a series of extracellular links, including a link at the tip that is composed of two cadherins, PCDH15 and CDH23, which interact to form a strong heterophilic complex (Kazmierczak et al., 2007). The lower end of the tip-link may bind to an as of yet unidentified mechanosensitive channel that opens in response to mechanical stimulation (Schwander et al., 2010). Both stereocilia tip-links and intermicrovillar links are involved in mediating adhesion between actin-based apical protrusions and are formed by a Ca^{2+}-dependent heterophilic complex of two structurally distinct cadherins. The stereocilia and intestinal protocadherins may also share unique structural similarities. CDH23 was found to possess a novel N-terminal Ca^{2+} binding site that PCDH24 might also possess (Elledge et al., 2010; Sotomayor et al., 2010). Moreover, genetic disruption of PCDH15 or CDH23 results in severe defects in stereocilia organization (Alagramam et al., 2011), whereas we have shown that knockdown of PCDH24 or MLPCDH disrupts BB assembly. One significant distinction between these two systems relates to the morphological end point: stereocilia assemble into a staircase pattern of graded height, whereas BB microvilli are strikingly uniform in length. Future studies must focus on understanding how seemingly similar adhesion-based mechanisms give rise to entirely different surface morphologies during differentiation.

Our studies also reveal a microvillus tip-localized protein complex with striking similarities to the Type 1 Usher syndrome protein interaction network, which includes CDH23, PCDH15, Myo7a, harmonin-b, and sans (Pan and Zhang, 2012). Usher syndrome is a major form of inherited deaf-blindness that impacts in 1 in 25,000 children and is caused by loss-of-function mutations in any of these components (Boughman et al., 1983). Type 1 Usher syndrome patients with mutations in harmonin can present with severe gastrointestinal symptoms including diarrhea with failure to thrive (Bitner-Glindzicz et al., 2000). However, the cellular basis of this pathology and the function of harmonin in the gut have not been studied. We find that harmonin targets specifically to the tips of BB microvilli where it promotes the enrichment of PCDH24 and MLPCDH. Moreover, harmonin KO mice harbor defects in BB organization along the length of the intestinal tract, a phenotype explained by the mistargeting of microvillar protocadherins and resulting loss of intermicrovillar adhesion. Because harmonin is localized specifically to microvillar tips, our findings may provide a basis for the intestinal phenotypes observed in Type 1 Usher syndrome patients.

Mechanism of microvillar tip enrichment

Based on our studies and previous work (Pan and Zhang, 2012), harmonin appears to serve as a central scaffold that mediates indirect interactions between membrane-associated cargoes and the cytoskeleton. Physical coupling of membrane-bound protocadherins to the actin core bundle, in this case through the actin-based motor Myo7b, could provide a mechanism for tip-directed transport or anchoring of fully formed adhesion complexes at microvillar tips. Although kinetic analyses indicate that Myo7b is high duty ratio (Henn and De La Cruz, 2005), more detailed studies on the dynamics of Myo7b in live cells will be

needed to determine the extent to which this motor functions in transport vs. anchoring of PCDH24 and MLPCDH.

In summary

The high packing density of BB microvilli is essential for the proper absorptive function of the intestinal mucosa. Perturbations in BB structure and reductions in microvillar density lead to nutrient malabsorption and osmotic diarrhea, common features of a number of GI diseases that pose significant threats to human health (Bailey et al., 1989; Khubchandani et al., 2011; Vallance et al., 2002). Our results provide significant insight on how the primary absorptive surface in the gut is formed and maintained, and highlight a pathway for crosstalk between luminal Ca^{2+} levels and BB assembly. Our observations also raise the possibility that formation of adhesion links between protrusions may be a conserved mechanism for refining apical surface architecture in diverse biological systems with unrelated functions. Although our studies focused on the intestinal epithelium, PCDH24 and MLPCDH are highly expressed in the kidney epithelium and could play a role in regulating BB assembly in that context as well. Interestingly, Ush1c patients do present with aminoaciduria and renal tubular dysfunction (Bitner-Glindzicz et al., 2000), and our initial studies suggest that MLCPDH is mislocalized in kidney tubule BBs from harmonin KO mice (data not shown). Future studies will build on the findings reported here by investigating the basis of intestinal pathologies characterized by perturbations to BB structure, and determining the extent to which other epithelial systems employ extracellular adhesion to organize cell surface architecture.

EXPERIMENTAL PROCEDURES

Cell Culture and lentiviral transduction

CACO-2_{BBE}, COS7, HEK293T and HEK293FT cells were cultured at 37°C and 5% CO_2 in DMEM with high glucose and 2 mM L-glutamine. Media was supplemented with 20% FBS for CACO-2_{BBE} cells and 10% FBS for COS7, HEK293T and HEK293FT cells. CACO-2_{BBE} stable cell lines were created using lentiviral transduction as follows. Lentivirus particles were generated by co-transfecting HEK293FT cells with KD or overexpression plasmids mixed with psPAX2 packaging and pMD2.G envelope plasmids using Fugene (Roche). Cells were subsequently incubated for two days to allow for lentiviral production. Media containing lentiviral particles was collected and filtered; particles were concentrated using the Lenti-X concentrator (Clontech). For lentivirus transduction, CACO-2_{BBE} cells were grown to 90% confluency and immediately before infection, growth media was exchanged to media containing polybrene. After 12 hrs of incubation with lentivirus, cells were allowed to recover and expand for 3 days. Cells were then shifted to media with puromycin or G418 to select for stable integration. Other details on the generation of all plasmids and stable cell lines used in this study are included in Extended Experimental Procedures.

Protein production, bead aggregation assays, and pull-down assays

Production of recombinant ectodomain was performed by transfection of HEK-293T cell cultures using Lipofectamine according to the manufacturer's protocol. Media containing

expressed protein was recovered, filtered, concentrated and used to label protein-A beads for bead aggregation assays or used directly in ectodomain pull-down assays. Bead aggregation assays were performed essentially as previously described (Emond et al., 2011). Protein pull-down assays involving harmonin, Myo7b, and the CD domains of the microvillar protocadherins were performed by co-transfection of epitope-tagged constructs into COS7 cells using Lipofectamine according to the manufacturer's protocol. After 48 hrs, cells were recovered, lysed and pull-downs performed using anti-FLAG M2 resin. Additional details are found in the Extended Experimental Procedures.

Microscopy

Cells and tissue sections were imaged using a Leica TCS SP5, a Zeiss LSM 710 META inverted laser-scanning confocal microscope, or a Leica SCN400 Slide scanner. Super-resolution microscopy was performed using a GE/Applied Precision DeltaVision OMX. SEM was performed using a Quanta 250 Environmental SEM operated in high vacuum mode with an accelerating voltage of 5-8 kV. TEM was performed on a Philips/FEI T-12 transmission electron microscope with an AMT CCD camera system. Images were contrast enhanced and cropped using ImageJ software (NIH). Details on sample preparation and data analysis are included in Extended Experimental Procedures.

Animal studies

Animal experiments were carried out in accordance with NIH Animal Care and Use Committee (DC009246) and Case Western Reserve University Institutional Animal Care and Use Committee guidelines.

Statistical Analysis

In all figures, error bars represent standard deviation. Unpaired *t test*s were used to determine statistical significance between reported values. Unless otherwise specified in the text, *n* values are reported in the figure legends for each condition measured.

Supplementary Material

Refer to Web version on PubMed Central for supplementary material.

Acknowledgments

The authors thank all members of the Tyska laboratory and the Vanderbilt Epithelial Biology Center for advice and support. Electron and light microscopy were performed in part through the use of the VUMC Cell Imaging Shared Resource. This work was supported by Intramural Programs of NIDCD, NIH (BK), American Heart Association (AHA) predoctoral fellowships (DAS, REM), AHA postdoctoral fellowship (SWC), AHA grant-in-aid 12GRNT12050314 (MJT), the VUMC Digestive Diseases Research Center (DK058404), a Vanderbilt University IDEAS award (MJT), and NIH DC009246 (QYZ), DK075555 and DK095811 (MJT).

REFERENCES

Alagramam KN, Goodyear RJ, Geng R, Furness DN, van Aken AF, Marcotti W, Kros CJ, Richardson GP. Mutations in protocadherin 15 and cadherin 23 affect tip links and mechanotransduction in mammalian sensory hair cells. PLoS One. 2011; 6:e19183. [PubMed: 21532990]

Bailey DS, Freedman AR, Price SC, Chescoe D, Ciclitira PJ. Early biochemical responses of the small intestine of coeliac patients to wheat gluten. Gut. 1989; 30:78–85. [PubMed: 2563983]

Belyantseva IA, Boger ET, Naz S, Frolenkov GI, Sellers JR, Ahmed ZM, Griffith AJ, Friedman TB. Myosin-XVa is required for tip localization of whirlin and differential elongation of hair-cell stereocilia. Nat Cell Biol. 2005; 7:148–156. [PubMed: 15654330]

Berndorff D, Gessner R, Kreft B, Schnoy N, Lajous-Petter AM, Loch N, Reutter W, Hortsch M, Tauber R. Liver-intestine cadherin: molecular cloning and characterization of a novel Ca(2+)-dependent cell adhesion molecule expressed in liver and intestine. J Cell Biol. 1994; 125:1353–1369. [PubMed: 8207063]

Bitner-Glindzicz M, Lindley KJ, Rutland P, Blaydon D, Smith VV, Milla PJ, Hussain K, Furth-Lavi J, Cosgrove KE, Shepherd RM, et al. A recessive contiguous gene deletion causing infantile hyperinsulinism, enteropathy and deafness identifies the Usher type 1C gene. Nat Genet. 2000; 26:56–60. [PubMed: 10973248]

Boeda B, El-Amraoui A, Bahloul A, Goodyear R, Daviet L, Blanchard S, Perfettini I, Fath KR, Shorte S, Reiners J, et al. Myosin VIIa, harmonin and cadherin 23, three Usher I gene products that cooperate to shape the sensory hair cell bundle. EMBO. 2002; J21:6689–6699.

Boggon TJ, Murray J, Chappuis-Flament S, Wong E, Gumbiner BM, Shapiro L. C-cadherin ectodomain structure and implications for cell adhesion mechanisms. Science. 2002; 296:1308–1313. [PubMed: 11964443]

Boller K, Vestweber D, Kemler R. Cell-adhesion molecule uvomorulin is localized in the intermediate junctions of adult intestinal epithelial cells. J Cell Biol. 1985; 100:327–332. [PubMed: 3880756]

Boughman JA, Vernon M, Shaver KA. Usher syndrome: definition and estimate of prevalence from two high-risk populations. J Chronic Dis. 1983; 36:595–603. [PubMed: 6885960]

Brasch J, Harrison OJ, Honig B, Shapiro L. Thinking outside the cell: how cadherins drive adhesion. Trends Cell Biol. 2012; 22:299–310. [PubMed: 22555008]

Burkel BM, von Dassow G, Bement WM. Versatile fluorescent probes for actin filaments based on the actin-binding domain of utrophin. Cell Motil Cytoskeleton. 2007; 64:822–832. [PubMed: 17685442]

Chan YH, Marshall WF. How cells know the size of their organelles. Science. 2012; 337:1186–1189. [PubMed: 22955827]

Chang J, Chance MR, Nicholas C, Ahmed N, Guilmeau S, Flandez M, Wang D, Byun DS, Nasser S, Albanese JM, et al. Proteomic changes during intestinal cell maturation in vivo. J Proteomics. 2008; 71:530–546. [PubMed: 18824147]

Chen ZY, Hasson T, Zhang DS, Schwender BJ, Derfler BH, Mooseker MS, Corey DP. Myosin-VIIb, a novel unconventional myosin, is a constituent of microvilli in transporting epithelia. Genomics. 2001; 72:285–296. [PubMed: 11401444]

D'Alterio C, Tran DD, Yeung MW, Hwang MS, Li MA, Arana CJ, Mulligan VK, Kubesh M, Sharma P, Chase M, et al. Drosophila melanogaster Cad99C, the orthologue of human Usher cadherin PCDH15, regulates the length of microvilli. J Cell Biol. 2005; 171:549–558. [PubMed: 16260500]

Elledge HM, Kazmierczak P, Clark P, Joseph JS, Kolatkar A, Kuhn P, Muller U. Structure of the N terminus of cadherin 23 reveals a new adhesion mechanism for a subset of cadherin superfamily members. Proc Natl Acad Sci U S A. 2010; 107:10708–10712. [PubMed: 20498078]

Emond MR, Biswas S, Blevins CJ, Jontes JD. A complex of Protocadherin-19 and N-cadherin mediates a novel mechanism of cell adhesion. J Cell Biol. 2011; 195:1115–1121. [PubMed: 22184198]

Ferrary E, Cohen-Tannoudji M, Pehau-Arnaudet G, Lapillonne A, Athman R, Ruiz T, Boulouha L, El Marjou F, Doye A, Fontaine JJ, et al. In vivo, villin is required for Ca(2+)-dependent F-actin disruption in intestinal brush borders. J Cell Biol. 1999; 146:819–830. [PubMed: 10459016]

Goldberg M, Peshkovsky C, Shifteh A, Al-Awqati Q. mu-Protocadherin, a novel developmentally regulated protocadherin with mucin-like domains. J Biol Chem. 2000; 275:24622–24629. [PubMed: 10801787]

Grati M, Kachar B. Myosin VIIa and sans localization at stereocilia upper tip-link density implicates these Usher syndrome proteins in mechanotransduction. Proc Natl Acad Sci U S A. 2011; 108:11476–11481. [PubMed: 21709241]

Grillet N, Xiong W, Reynolds A, Kazmierczak P, Sato T, Lillo C, Dumont RA, Hintermann E, Sczaniecka A, Schwander M, et al. Harmonin mutations cause mechanotransduction defects in cochlear hair cells. Neuron. 2009; 62:375–387. [PubMed: 19447093]

Grimm-Gunter EM, Revenu C, Ramos S, Hurbain I, Smyth N, Ferrary E, Louvard D, Robine S, Rivero F. Plastin 1 binds to keratin and is required for terminal web assembly in the intestinal epithelium. Mol Biol Cell. 2009; 20:2549–2562. [PubMed: 19321664]

Guillot C, Lecuit T. Mechanics of epithelial tissue homeostasis and morphogenesis. Science. 2013; 340:1185–1189. [PubMed: 23744939]

Henn A, De La Cruz EM. Vertebrate myosin VIIb is a high duty ratio motor adapted for generating and maintaining tension. J Biol Chem. 2005; 280:39665–39676. [PubMed: 16186105]

Jeejeebhoy KN. Short bowel syndrome: a nutritional and medical approach. CMAJ. 2002; 166:1297–1302. [PubMed: 12041848]

Kazmierczak P, Sakaguchi H, Tokita J, Wilson-Kubalek EM, Milligan RA, Muller U, Kachar B. Cadherin 23 and protocadherin 15 interact to form tip-link filaments in sensory hair cells. Nature. 2007; 449:87–91. [PubMed: 17805295]

Khubchandani SR, Vohra P, Chitale AR, Sidana P. Microvillous inclusion disease?an ultrastructural diagnosis: with a review of the literature. Ultrastruct Pathol. 2011; 35:87–91. [PubMed: 21299349]

Kobayashi I, Imamura K, Kubota M, Ishikawa S, Yamada M, Tonoki H, Okano M, Storch WB, Moriuchi T, Sakiyama Y, et al. Identification of an autoimmune enteropathy-related 75-kilodalton antigen. Gastroenterology. 1999; 117:823–830. [PubMed: 10500064]

Mariadason JM, Nicholas C, L'Italien KE, Zhuang M, Smartt HJ, Heerdt BG, Yang W, Corner GA, Wilson AJ, Klampfer L, et al. Gene expression profiling of intestinal epithelial cell maturation along the crypt-villus axis. Gastroenterology. 2005; 128:1081–1088. [PubMed: 15825089]

Maroux S, Coudrier E, Feracci H, Gorvel JP, Louvard D. Molecular organization of the intestinal brush border. Biochimie. 1988; 70:1297–1306. [PubMed: 3147722]

McConnell RE, Benesh AE, Mao S, Tabb DL, Tyska MJ. Proteomic analysis of the enterocyte brush border. Am J Physiol Gastrointest Liver Physiol. 2011; 300:G914–926. [PubMed: 21330445]

Mooseker MS. Organization, chemistry, and assembly of the cytoskeletal apparatus of the intestinal brush border. Ann Rev Cell Biol. 1985; 1:209–241. [PubMed: 3916317]

Mukherjee S, Vaishnava S, Hooper LV. Multi-layered regulation of intestinal antimicrobial defense. Cell Mol Life Sci. 2008; 65:3019–3027. [PubMed: 18560756]

Nelson WJ, Veshnock PJ. Ankyrin binding to (Na+ + K+)ATPase and implications for the organization of membrane domains in polarized cells. Nature. 1987; 328:533–536. [PubMed: 3039371]

Nose A, Tsuji K, Takeichi M. Localization of specificity determining sites in cadherin cell adhesion molecules. Cell. 1990; 61:147–155. [PubMed: 2317870]

Pan L, Zhang M. Structures of usher syndrome 1 proteins and their complexes. Physiology (Bethesda). 2012; 27:25–42.

Peterson MD, Mooseker MS. Characterization of the enterocyte-like brush border cytoskeleton of the C2BBe clones of the human intestinal cell line, Caco-2. J Cell Sci. 1992; 102:581–600. [PubMed: 1506435]

Revenu C, Ubelmann F, Hurbain I, El-Marjou F, Dingli F, Loew D, Delacour D, Gilet J, Brot-Laroche E, Rivero F, et al. A new role for the architecture of microvillar actin bundles in apical retention of membrane proteins. Mol Biol Cell. 2012; 23:324–336. [PubMed: 22114352]

Saotome I, Curto M, McClatchey AI. Ezrin is essential for epithelial organization and villus morphogenesis in the developing intestine. Dev Cell. 2004; 6:855–864. [PubMed: 15177033]

Schlichting K, Wilsch-Brauninger M, Demontis F, Dahmann C. Cadherin Cad99C is required for normal microvilli morphology in Drosophila follicle cells. J Cell Sci. 2006; 119:1184–1195. [PubMed: 16507588]

Schwander M, Kachar B, Muller U. Review series: The cell biology of hearing. J Cell Biol. 2010; 190:9–20. [PubMed: 20624897]

Selsted ME, Ouellette AJ. Mammalian defensins in the antimicrobial immune response. Nat Immunol. 2005; 6:551–557. [PubMed: 15908936]

Shifrin DA Jr. Tyska MJ. Ready...aim...fire into the lumen: a new role for enterocyte microvilli in gut host defense. Gut Microbes. 2012; 3:460–462. [PubMed: 22825496]

Siemens J, Kazmierczak P, Reynolds A, Sticker M, Littlewood-Evans A, Muller U. The Usher syndrome proteins cadherin 23 and harmonin form a complex by means of PDZ-domain interactions. Proc Natl Acad Sci U S A. 2002; 99:14946–14951. [PubMed: 12407180]

Sotomayor M, Weihofen WA, Gaudet R, Corey DP. Structural determinants of cadherin-23 function in hearing and deafness. Neuron. 2010; 66:85–100. [PubMed: 20399731]

Sotomayor M, Weihofen WA, Gaudet R, Corey DP. Structure of a force-conveying cadherin bond essential for inner-ear mechanotransduction. Nature. 2012; 492:128–132. [PubMed: 23135401]

Tian C, Liu XZ, Han F, Yu H, Longo-Guess C, Yang B, Lu C, Yan D, Zheng QY. Ush1c gene expression levels in the ear and eye suggest different roles for Ush1c in neurosensory organs in a new Ush1c knockout mouse. Brain Res. 2010; 1328:57–70. [PubMed: 20211154]

Tyska MJ, Mackey AT, Huang JD, Copeland NG, Jenkins NA, Mooseker MS. Myosin-1a is critical for normal brush border structure and composition. Mol Biol Cell. 2005; 16:2443–2457. [PubMed: 15758024]

Tyska MJ, Mooseker MS. A role for myosin-1A in the localization of a brush border disaccharidase. J Cell Biol. 2004; 165:395–405. [PubMed: 15138292]

Vallance BA, Chan C, Robertson ML, Finlay BB. Enteropathogenic and enterohemorrhagic Escherichia coli infections: emerging themes in pathogenesis and prevention. Can J Gastroenterol. 2002; 16:771–778. [PubMed: 12464970]

Verpy E, Leibovici M, Zwaenepoel I, Liu XZ, Gal A, Salem N, Mansour A, Blanchard S, Kobayashi I, Keats BJ, et al. A defect in harmonin, a PDZ domain-containing protein expressed in the inner ear sensory hair cells, underlies Usher syndrome type 1C. Nat Genet. 2000; 26:51–55. [PubMed: 10973247]

Widmark JM. Imaging-related medications: a class overview. Proc (Bayl Univ Med Cent). 2007; 20:408–417. [PubMed: 17948119]

- Packing of brush border microvilli is driven by adhesion between protrusion tips
- Intermicrovillar adhesion complexes are composed of PCDH24 and MLPCDH
- PCDH24 and MLPCDH target to microvillar tips via interactions with harmonin and Myo7b
- Mice lacking harmonin exhibit defects in brush border assembly

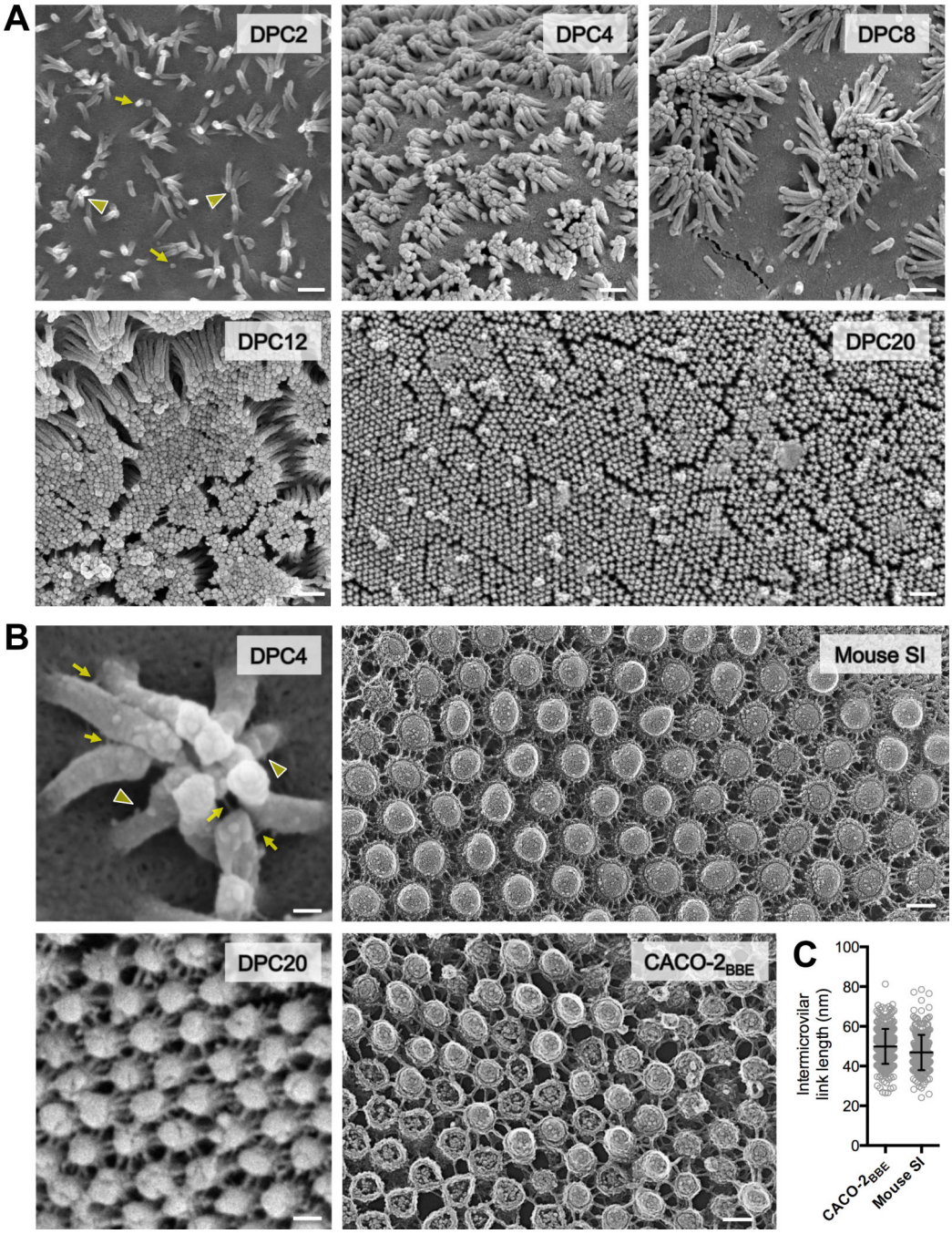

Figure 1. Enterocyte BB microvilli cluster during differentiation and are connected by thread-like links

(A) SEM of CACO-2_{BBE} cells from a differentiation time series; days post confluency (DPC) are indicated. Yellow arrows point to initial microvillar membrane buds, arrowheads to distal tip contact of longer microvilli. Scale bars, 500 nm. (B) High magnification images of CACO-2_{BBE} cells and native intestinal tissue. *Left upper*: SEM of a microvillar cluster from 4-DPC CACO-2_{BBE} cell. Yellow arrows point to intact intermicrovillar adhesion links, arrowheads to unpaired or broken links. *Left bottom*: SEM of a 20-DPC CACO-2_{BBE} monolayer. *Right upper*: Freeze-etch EM of the BB from mouse small intestinal tissue. *Right lower*: Freeze-etch EM of the BB from 20-DPC CACO-2_{BBE} cells. Scale bars, 100 nm. (C) Intermicrovillar link lengths from CACO-2_{BBE} and mouse intestinal tissue freeze-etch EM images (mean ± SD). See also Figure S1.

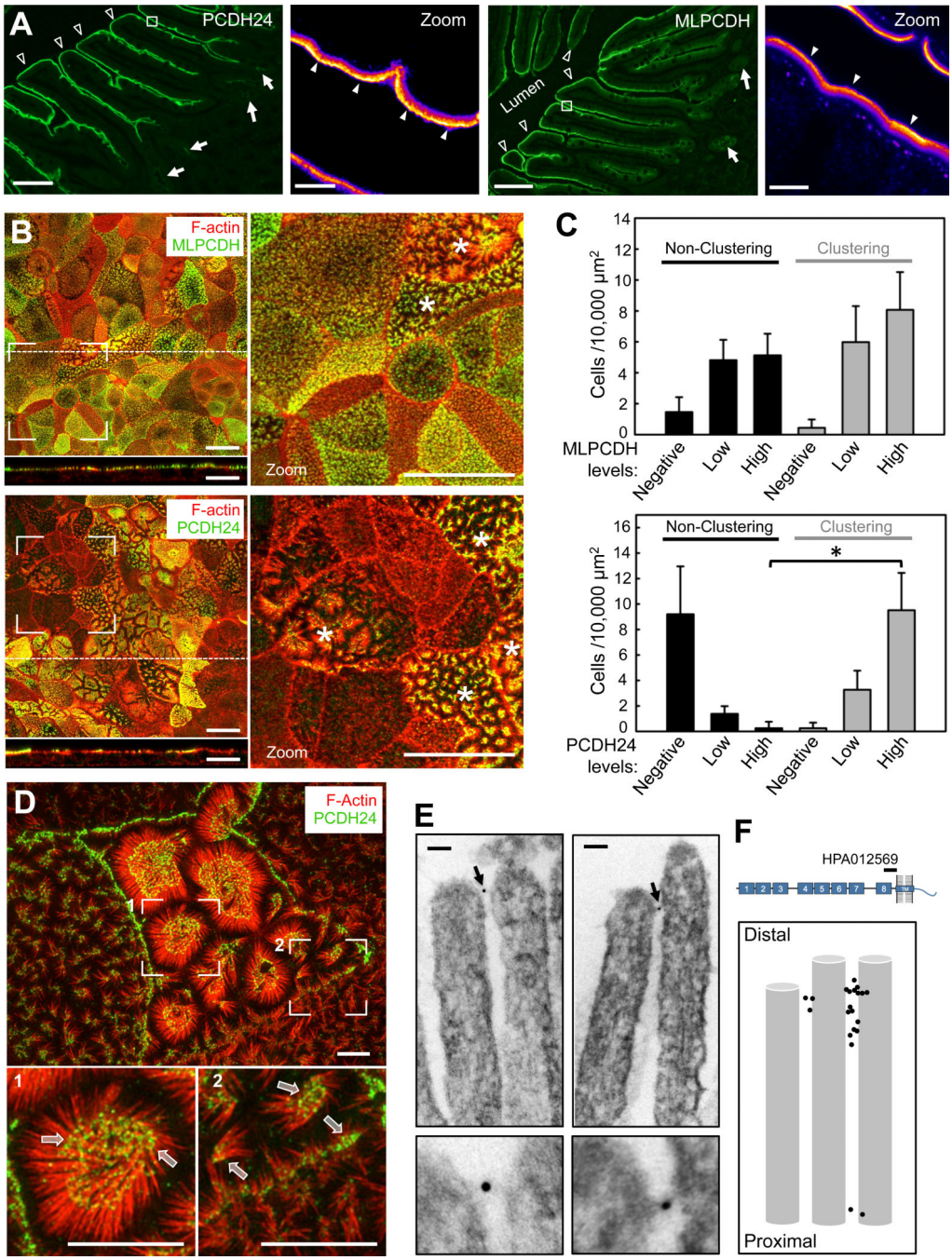

Figure 2. MLPCDH and PCDH24 localize to the BB in both native intestinal tissue and CACO-2$_{BBE}$ monolayers

(A) Confocal microscopy of human duodenal tissue stained for PCDH24 and MLPCDH. Arrows point to intestinal crypts, open arrowheads to villi, filled arrowheads to the enrichment of PCDH24 and MLPCDH at the distal tips of the microvilli. Boxed regions denote zoomed heat map images of the BB. Scale bars, 100 µm; *zoom*, 5 µm. (B) Confocal images of 12-DPC cells stained for F-actin and either MLPCDH (*top*) or PCDH24 (*bottom*). Dashed lines represent where x-z sections were taken (shown below the *en face* images). Asterisks denote cells undergoing robust microvillar clustering. Scale bars, 20 µm. (C) Microvillar clustering as a function of endogenous expression levels of MLPCDH (*top*; n = 995 cells) or PCDH24 (*bottom*; n = 1146 cells) in 12-DPC monolayers (mean ± SD). *p < 0.0001, *t* test. (D) Super-resolution microscopy of 12-DPC cells stained

for F-actin and PCDH24. Outlined arrows point to distal tip enrichment of PCDH24 in clustering microvilli. Scale bars, 5 μm. (E) Immuno-gold TEM of PCDH24-labeled 12-DPC cells. *Bottom* panels show zoomed image of highlighted gold particles. Scale bars, 50 nm. (F) Relative positions of gold-labeled particles along the microvillar axis. See also Figure S2.

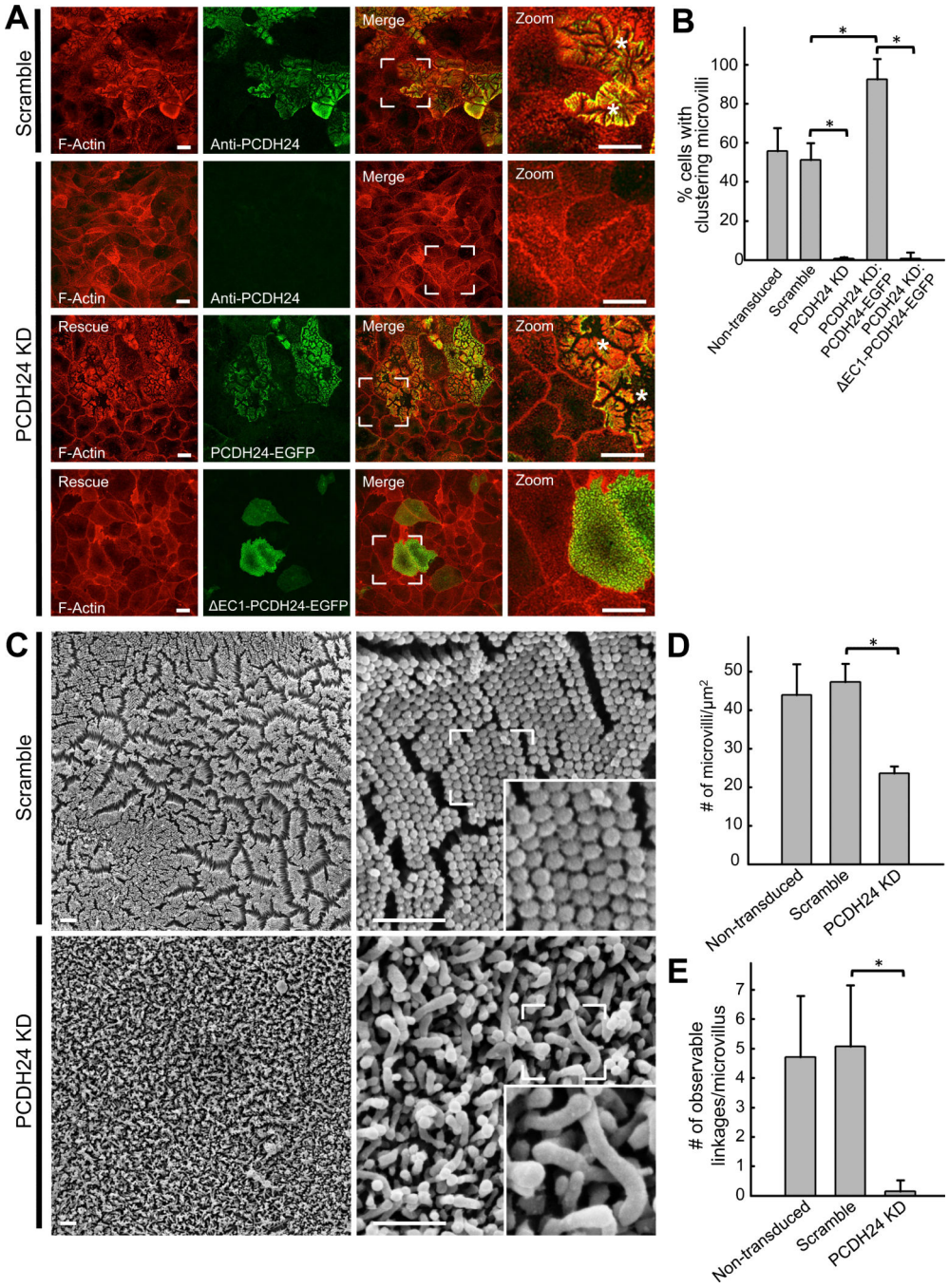

Figure 3. Stable shRNA knockdown of PCDH24 in CACO-2$_{BBE}$ cells abolishes microvillar clustering and disrupts BB formation

(A) Confocal images of 12-DPC cells stably expressing either a scramble shRNA construct or an shRNA targeting PCDH24. Scramble and PCDH24 KD cells have been stained for F-actin and PCDH24, while PCDH24 KD cell lines expressing rescue constructs have been stained for F-actin only. Asterisks denote cells undergoing robust microvillar clustering. Scale bars, 15 μm (B) Microvillar clustering in non-transduced, scramble, PCDH24 KD, and PCDH24 rescue cell lines. For quantification of rescue lines, only EGFP-positive cells were scored (mean ± SD). Non-transduced cells n = 2639, scramble control cells n = 1019, PCDH24 KD cells n = 1056, PCDH24 KD rescue PCDH24-EGFP n = 115, PCDH24 KD rescue ΔEC1 PCDH24-EGFP cells n = 160; *p values < 0.0001, *t* test. (C) SEM images of 20-DPC CACO-2$_{BBE}$ cells stably expressing either a scramble

shRNA construct (*top*) or an shRNA targeting PCDH24 (*bottom*). Scale bars, 1 μm. (D) Microvillar packing density in non-transduced, scramble and PCDH24 KD stably transduced 20-DPC cells (mean ± SD). Area quantified and number of microvilli counted: non-transduced cells area = 150 μm^2, microvilli n = 6599; scramble cells area = 125 μm^2, microvilli n = 5919; PCDH24 KD cells area = 225 μm^2, cells microvilli n = 5318; *p value < 0.0001, *t* test. (E) Observable links at the distal tips of microvilli in non-transduced, scramble and PCDH24 KD cell lines. Microvilli counted from non-transduced cells n = 100, scramble control cells n = 94 and PCDH24 KD cells n = 110; *p value < 0.0001, *t* test. See also Figure S3.

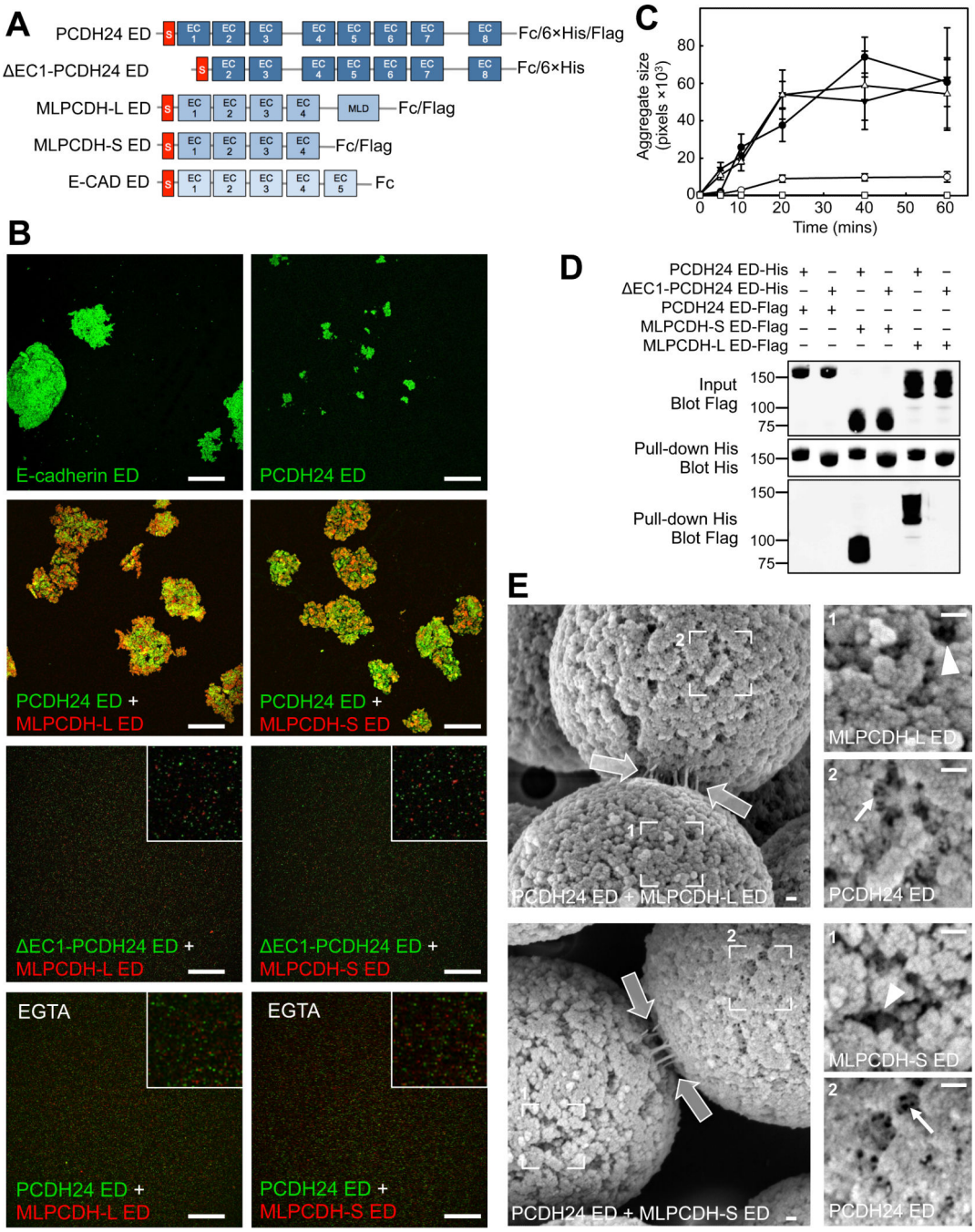

Figure 4. PCDH24 and MLPCDH interact to form Ca^{2+}-dependent *trans* heterophilic adhesion complexes

(A) Constructs used in bead aggregation and pull-down assays. The signal sequences (S) of the cadherin EDs are shown in red. The long isoform of MLPCDH contains a juxtamembrane mucin-like repeat domain (MLD). (B) Confocal images of ED-coated fluorescent bead aggregation assays at the 60 min time point. Insets shown in selected panels are zoomed images to show the presence of individual beads. Scale bars, 250 μm. (C) Bead aggregate size as a function of time. n=three independent experiments. (D) Pull-down analysis using the EDs of PCDH24 and both isoforms of MLPCDH. (E) SEM images of *in vitro* reconstituted *trans* heterophilic adhesion complexes between beads coated with the ED of PCDH24 and either MLPCDHL (*top*) or MLPCDH-S (*bottom*). White outlined arrows point to adhesion links at bead-bead interfaces. Box 1 (*right upper*) confirms

the identity of the denoted beads as being coated with MLPCDH ED isoforms, given the lack of intra-bead bonds (see arrowheads). Box 2 (*right lower*) shows PCDH24-coated beads that possess an extensive network of intra-bead bonds (see arrows). Scale bars, 100 nm. See also Figure S4.

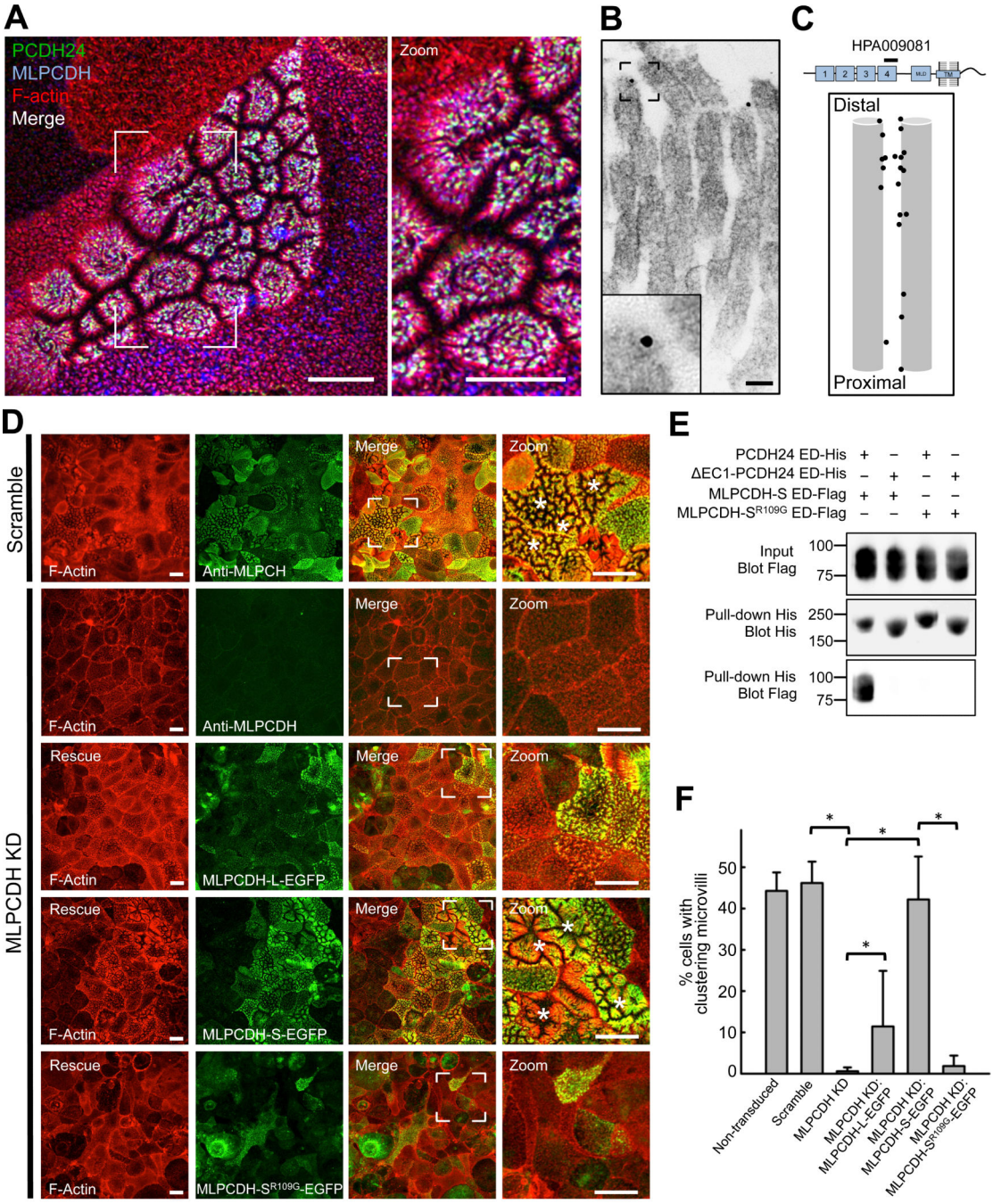

Figure 5. MLPCDH colocalizes with PCDH24 and is necessary for microvillar clustering in CACO-2$_{BBE}$ cells

(A) Confocal microscopy of 12-DPC CACO-2$_{BBE}$ monolayers stained for PCDH24, MLPCDH and F-actin. Scale bars, 10 μm. (B) Immuno-gold TEM of MLPCDH-labeled 12-DPC CACO-2$_{BBE}$ cells. *Inset* shows a zoomed image of a gold particle. Scale bar, 50 nm. (C) Relative positions of gold-labeled particles along the microvillar axis. (D) Confocal images of 12-DPC CACO-2$_{BBE}$ cells stably expressing either a scramble shRNA construct or an shRNA targeting MLPCDH. Scramble and MLPCDH KD cells have been stained for F-actin and MLPCDH, while MLPCDH KD cell lines expressing rescue constructs have been stained for F-actin and GFP. Asterisks denote cells undergoing robust microvillar clustering. Scale bars, 15 μm (E) Pull-down analysis of the MLPCDH-S^{R109G} mutant ED interaction with the PCDH24 ED. (F) Microvillar clustering in non-

transduced, scramble, MLPCDH KD, and MLPCDH rescue CACO-2_{BBE} cell lines. For quantification of rescue cell lines, only EGFP-positive cells were scored (mean ± SD). Non-transduced cells n = 1857, scramble control cells n = 963, MLPCDH KD cells n = 1324, MLPCDH KD rescue MLPCDH-L-EGFP n = 441, MLPCDH KD rescue MLPCDH-S-EGFP n = 1141, MLPCDH KD rescue MLPCDH-S^{R109G}-EGFP cells n = 520; *p values < 0.0001, *t* test. See also Figure S3.

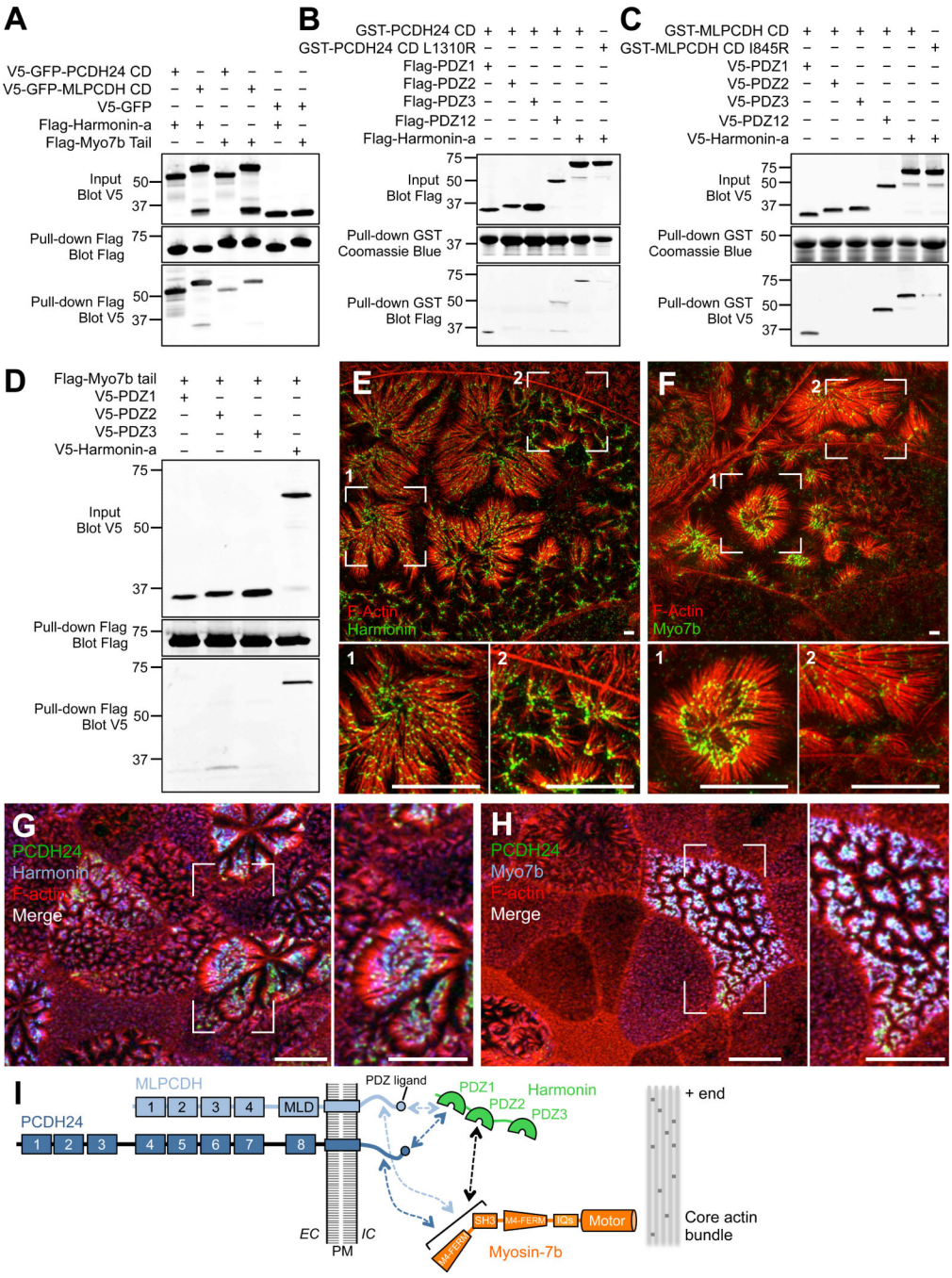

Figure 6. Microvillar protocadherins form a complex with harmonin and Myo7b at the tips of BB microvilli

(A) Pull-down analysis of the interactions of the CDs of PCDH24 and MLPCDH with harmonin-a and the cargo-binding tail of Myo7b. (B and C) Mapping the domains of harmonin-a that interact with the CDs of PCDH24 and MLPCDH. (D) Mapping the domain of harmonin-a that interacts with Myo7b. (E and F) Super-resolution microscopy of 12-DPC CACO-2_{BBE} cells stained for F-actin and harmonin or Myo7b. Scale bars, 3 μm. (G and H) Confocal microscopy of 12-DPC CACO-2_{BBE} cells stained for PCDH24, F-actin, and harmonin or Myo7b. Scale bars, 10 μm. (I) Cartoon summary of interactions between the CDs of microvillar protocadherins, harmonin and Myo7b. See also Figure S6.

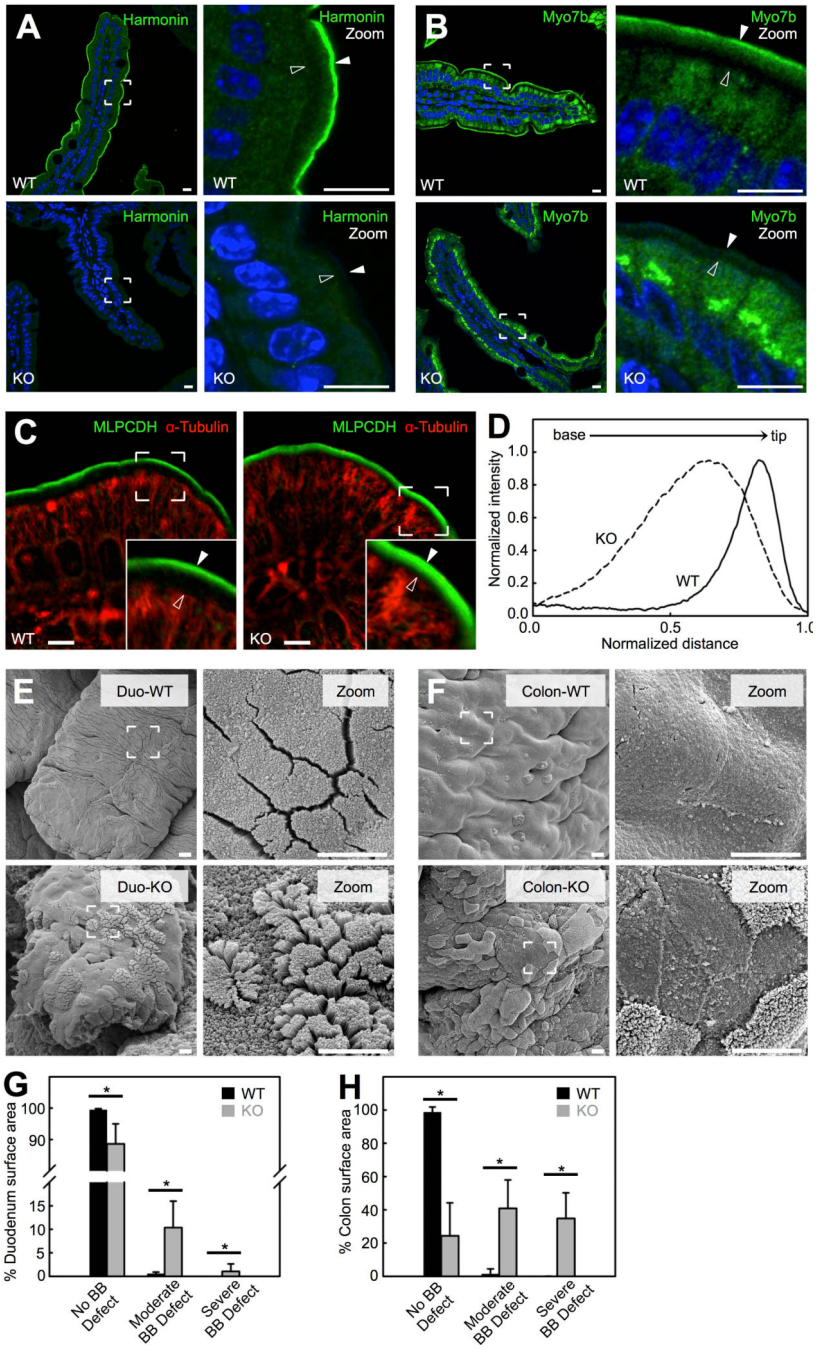

Figure 7. Harmonin KO mice exhibit defects in BB morphology

(A and B) Confocal images of villi from WT (*top*) and harmonin KO (*bottom*) stained for harmonin, Myo7b and DAPI (blue). Boundaries of the BB are denoted with filled arrowheads (microvillar tips) and open arrowheads (terminal web) in the zoomed images (*right panels*). Scale bars, 10 μm. (C) Confocal images of villi from WT (*left*) and harmonin KO (*right*) littermates stained for MLPCDH and α-tubulin. In zoomed images microvillar tips are marked with filled arrowheads and the terminal web is marked with open arrowheads (*insets*). Scale bars, 5 μm. (D) Line scans of MLPCDH immunofluorescence intensity within the BB of WT and harmonin KO. (E) SEM images of the apical surface of villi from the duodenum (Duod) of WT (*top*) and harmonin KO (*bottom*). (F) SEM of the proximal colon apical surface from WT (*top*) and harmonin KO (*bottom*) mice. Scale

bars, 5 μm. (G and H) Degree of BB defects exhibited in the duodenum (G) and colon (H) of WT and harmonin KO (mean ± SD). No BB defect was defined as an apical surface that possessed well-packed microvilli of uniform length; moderate BB defect as apical microvilli that were disheveled in appearance; severe BB defect as areas that lacked microvilli. Surface area measured: WT SI = 4,001,746 μm^2, Harmonin KO SI = 296,867 μm^2, WT colon = 511,465 μm^2, Harmonin KO colon = 975,557 μm^2; n = 4 animals for each genotype. *p value < 0.0001, *t* test. See also Figure S7.